Scripta Materialia 182 (2020) 32–37

Contents lists available at ScienceDirect

Scripta Materialia

journal homepage: www.elsevier.com/locate/scriptamat

Relaxation and crystallization studied by observing the surface morphology evolution of atomically flat $Pt_{57.5}Cu_{14.7}Ni_{5.3}P_{22.5}$ upon annealing

Zheng Chen[a], Amit Datye[a], Jittisa Ketkaew[a], Sungwoo Sohn[a], Chao Zhou[a], Omur E. Dagdeviren[a], Jan Schroers[a], Udo D. Schwarz[a,b,*]

[a] Department of Mechanical Engineering and Materials Science, Yale University, New Haven, CT 06511, USA
[b] Department of Chemical and Environmental Engineering, Yale University, New Haven, CT 06511, USA

ARTICLE INFO

Article history:
Received 7 February 2020
Accepted 21 February 2020

Keywords:
Bulk metallic glass
Relaxation
Crystallization
Atomic force microscopy
Annealing

ABSTRACT

The evolution of the surface morphology of $Pt_{57.5}Cu_{14.7}Ni_{5.3}P_{22.5}$ bulk metallic glasses thermoplastically formed by replication of $SrTiO_3$ single crystals during heat treatments is investigated by atomic force microscopy. Due to the unique imprinting process, the surface of the bulk metallic glass features a terraced structure with sub-angstrom surface roughness. Upon heating over the material's glass transition temperature, the surface rearranges and relaxes towards a more stable, denser packed glass by smoothening out steps and increasing on-terrace surface roughness. With further increasing annealing temperatures, substantial surface alterations are observed because of increased arrangement kinetics and the onset of crystallization.

Metallic glasses lack long-range order, which provides them with properties distinct from what crystalline materials exhibit [1,2]. Among metallic glasses, bulk metallic glasses (BMGs) exhibit particularly high crystallization resistance with critical cooling rates below 1000 K/s [3], offering often large supercooled liquid regions and a high suitability for thermoplastic forming (TPF) [4–10]. As a consequence, one can not only fabricate large objects with almost unlimited shapes [7,9,11–13], but thanks to the absence of an intrinsic size limit beyond the existence of atoms, these objects can also feature extremely fine substructures. Thus far, TPF has yielded structures from the centimeter to the atomic scale [8,14–16].

The properties of BMGs can be tuned by setting the glass' degree of relaxation, and establishing the related preparation-structure-property relationships has become a key focus of many studies [17–24]. Thereby, the degree of relaxation is mostly set by a combination of time and temperature during annealing, which ultimately launches the crystallization process occurring at ≈1000 × of the time scale of structural relaxation [25]. As a result, nanocrystals may be embedded within an amorphous matrix, causing changes in the specimen's properties [26,27]. Since the atomic structure of BMGs is difficult to directly observe, experimental efforts have mainly concentrated on uncovering correlations between properties such as Young's modulus, hardness, viscosity, enthalpy, and density, which provide indirect access to understanding the relaxation process [17,21,28–30]. Here, we present an alternate approach to explore the effect of relaxation and crystallization through the high-resolution imaging of surface morphology changes induced by heating using atomic force microscopy (AFM).

Due to their promise of providing high-resolution surface maps without requiring long-range order, scanned probe methods have been applied to image the surfaces of disordered systems as early as 1986 [31–33]. However, despite a sizeable number of studies published, results only show 'hilly' surfaces with a surface corrugation of ≳1 nm, and no atomic resolution has been achieved unless samples were crystallized by heating [34–42]. Interpreted as reflecting the cluster-packing nature of the glasses [43–48], the occurrence of these 'hills' is, however, detrimental to the reliable extraction of the mechanisms driving the evolution of the material's surface structure upon annealing.

To understand why better insight has not been achieved in the past, it is instructive to recall what options exist to prepare well-defined surfaces. Crystalline samples are commonly prepared in ultrahigh vacuum by cycles of sputtering and annealing: Sputtering removes surface contamination but roughens the surface, while subsequent annealing allows the cleaned crystal to reach a state

* Corresponding author at: Department of Mechanical Engineering and Materials Science, Yale University, New Haven, CT 06511, USA.
E-mail address: udo.schwarz@yale.edu (U.D. Schwarz).

https://doi.org/10.1016/j.scriptamat.2020.02.035
1359-6462/

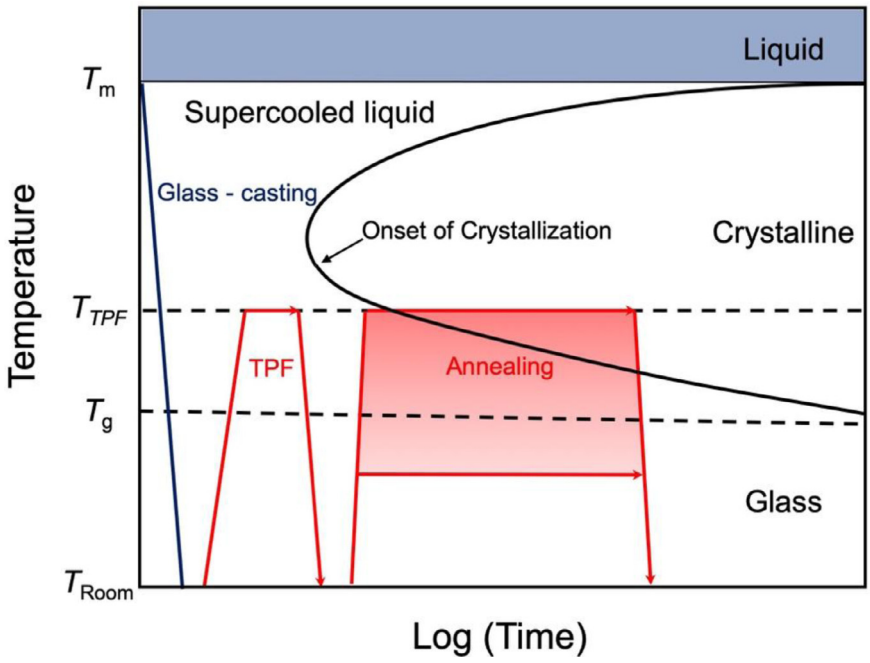

Fig. 1. Schematic time-temperature-transformation diagram visualizing the thermal treatment of samples used in this study (T_m = melting temperature of the alloy; T_{Room} = room temperature). Samples are annealed within the regime covered by the red-shaded area, which has been set so that the sample heated to the lowest temperature (210 °C) remain virtually unaffected by the processing while the sample exposed to the highest temperature (270 °C) has almost completely crystallized. (For interpretation of the references to color in this figure legend, the reader is referred to the web version of this article.)

of low surface energy, usually by forming large, atomically flat terraces. If applied to amorphous alloys, however, annealing will not lead to satisfactorily flat surfaces unless heated so high that crystallization occurs. As a consequence, the minimum achievable surface roughness is dependent on the quality of ex-situ treatment methods such as grinding and polishing [40–42].

Here, we avoid the challenges posed by excessive surface roughness on data analysis by preparing samples from $Pt_{57.5}Cu_{14.7}Ni_{5.3}P_{22.5}$ to feature surfaces terminated by virtually atomically flat terraces [16], which are then used to track the evolution of the material's surface morphology upon annealing with unprecedented detail. Through comparing AFM images before and after annealing at the exact same locations, we find that when the samples are being heated just below T_g, the material stays amorphous, but reacts by smoothening out steps while increasing on-terrace roughness. In contrast, treatment above T_g induces more substantial changes, which are, despite still being significantly below temperatures commonly associated with crystallization, at least in part linked to the onset of crystallization.

The $Pt_{57.5}Cu_{14.7}Ni_{5.3}P_{22.5}$ alloy ('Pt-BMG') used for the experiments is known to have excellent glass forming ability while being highly processable [49]. From the as-cast alloy, samples featuring virtually atomically flat surfaces with sub-angstrom root mean square (RMS) roughness within terraces are produced by thermoplastic forming as described in detail elsewhere [16] using $SrTiO_3$ ('STO') single crystals as molds. In short, (100)-oriented STO crystals from MTI Corporation (Richmond, CA) are heated in air under oxygen flow at 1000 °C for two hours, which results in a well-defined surface morphology with terraces of ≈50–300 nm width that are separated by one-unit-cell high steps (3.9 Å). For the imprinting, the STO is introduced into a specially designed press and an as-cast Pt-BMG ingot is placed on top of it. Both are then heated to T_{TPF} = 270 °C before the pressure is ramped up within three minutes to ≈10 MPa, at which the BMG/STO stack is kept for an additional three minutes before the pressure is released. The thermal mismatch between the substrate and the sample then causes the formed Pt-BMG disc of ≈1 cm diameter to separate from the STO upon cooling. The surface of the Pt-BMG replica that was in contact with the STO mold precisely mirrors the STO's atomically flat terraced surface, including sharing its step height.

For such imprinted samples, differential scanning calorimetry (DSC) was carried out using a Perkin Elmer Diamond machine through ramping the temperature by 20 K/min revealed a T_g of 234 °C, an 'onset of crystallization' temperature T_x of 275 °C, and a temperature T_p of 293 °C denoting the peak's maximum value. In addition, DSC experiments showed that if heated at a constant temperature of 270 °C instead, crystallization starts after ≈5 min with the samples being >95% crystalline after 20 min. In contrast, samples annealed at 250 °C do not measurably crystallize for ≈1 h while they are ≈30% crystalline after 2 h and >95% crystalline after 6 h. For the AFM experiments, freshly imprinted samples are annealed for 20 min each at different temperatures from 210 to 270 °C inside the DSC machine with high purity argon gas flow to prevent surface oxidation, with a room temperature sample kept for reference. Using this protocol, samples annealed at 210 °C remain virtually unaltered while the ones exposed to 270 °C are expected to be almost completely crystallized (see Fig. 1). All samples are cut from the same imprinted Pt-based BMG disc, which ensures that they share the same composition and thermal history before the annealing. AFM images are acquired before and after the heat treatments at the same locations using a Bruker Multimode AFM with Nanoscope III electronics (Bruker, Santa Barbara, CA) and PPP-NCL-50 silicon cantilevers (Nanosensors, Neuchâtel, Switzerland) in tapping mode.

The AFM images shown in Fig. 2(a)–(h) illustrate the general trend of surface changes after annealing at different temperatures, with the initially well-defined terrace structures getting blurred as the temperature increases from 210 °C to 240 °C. Starting at 250 °C, all terraces disappear and new structures are formed that become larger and larger as the temperature is increased up to 270 °C. This is analyzed in more details in Fig. 2(i)–(k), which depict height profiles taken from the samples heated to 250 °C, 260 °C, and

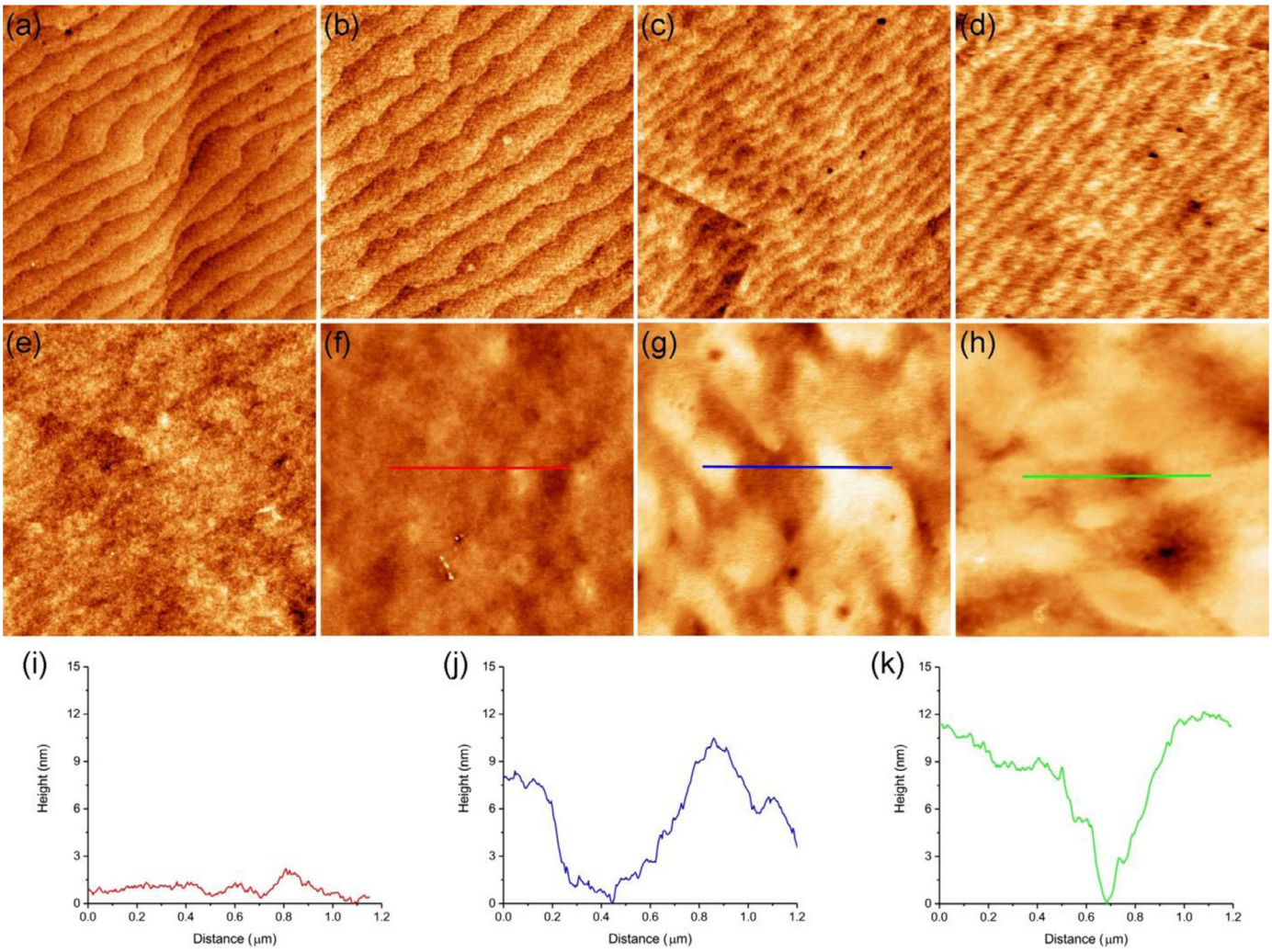

Fig. 2. Representative images of Pt-BMG samples, prepared as described in the text through thermoplastic forming to feature atomically flat terraces separated by steps of 3.9 Å height before annealing [16], after heat treatment at (b) 210 °C, (c) 220 °C, (d) 230 °C, (e) 240 °C, (f) 250 °C, (g) 260 °C and (h) 270 °C for 20 min in argon gas. The sample shown in (a) was exposed to the Ar gas as well, but without heating. Image size is 2 μm × 2 μm in all panels. (i)–(k) Height profiles taken along the locations identified by the lines of identical color in panels (f)–(h). It can be seen that the corrugation increases significantly upon heating at higher temperatures. (For interpretation of the references to color in this figure legend, the reader is referred to the web version of this article.)

270 °C. From these profiles, we see that the corrugation of the sample annealed at 250 °C is around 2 nm, but dramatically increases to 10 nm and larger for the samples kept at 260 °C and 270 °C.

At temperatures of 240 °C and lower, changes in surface appearance are subtler, which is why we turn to Fig. 3 for a more in-depth analysis. The two images shown in each panel on the left were captured at identical locations, but before and after the thermal treatment was carried out. Height profiles along the lines indicated in the before and after images are then shown on the right-hand side. While there is very little change visible in Fig. 3(a) and (b), Fig. 3(c) exposes that the sharpness at the terrace edges is lower after being annealed at 230 °C. For better visualization of this effect, we have added the black-and-white pictures in the upper right of each panel, which represents the differential obtained by subtracting the before and after images. While being almost featureless in (a), increasingly broader 'white stripes' around the locations of the step edges in (b) and (c) reflect the tendency of the surface to 'smoothen' its step edges. The red curve in Fig. 3(d) and the corresponding differential image finally reveal that the surface eventually loses most of its stepped structure through heating. Instead, it becomes more like a tilted plane with random fluctuations that are markedly different from the angular shape the blue curve follows before the roughening of Fig. 2(f)–(h) kicks in.

To further investigate the tendency to 'smoothen' step edges, an analysis of the root mean square (RMS) surface roughness values obtained after the different preparation procedures has been undertaken. Thereby, we define the ratio of the RMS roughness obtained *after* heat treatment to the value it had on the exact same location *before* the heat treatment as 'roughness ratio'. Comparing this value to 1.00, which would indicate no change in roughness, allows to quantify the degree of change that has occurred during annealing. For better insight, we introduce two different roughness ratios: an 'overall ratio' that compares entire AFM images of the same size that have been imaged at the same location before and after heat treatment, and an 'on-terrace ratio' representing a comparison of the surface roughness on an individual terrace only. As a consequence, the overall ratio averages the effect of many step edges on roughness while the on-terrace ratio only focuses on what is happening within an area that is virtually atomically flat at the onset of heating. Representative areas for obtaining one value for this on-terrace ratio are shown with the two black squares in Fig. 3(a). The areas within squares used for determining on-terrace roughness determinations were, due to the small width of the

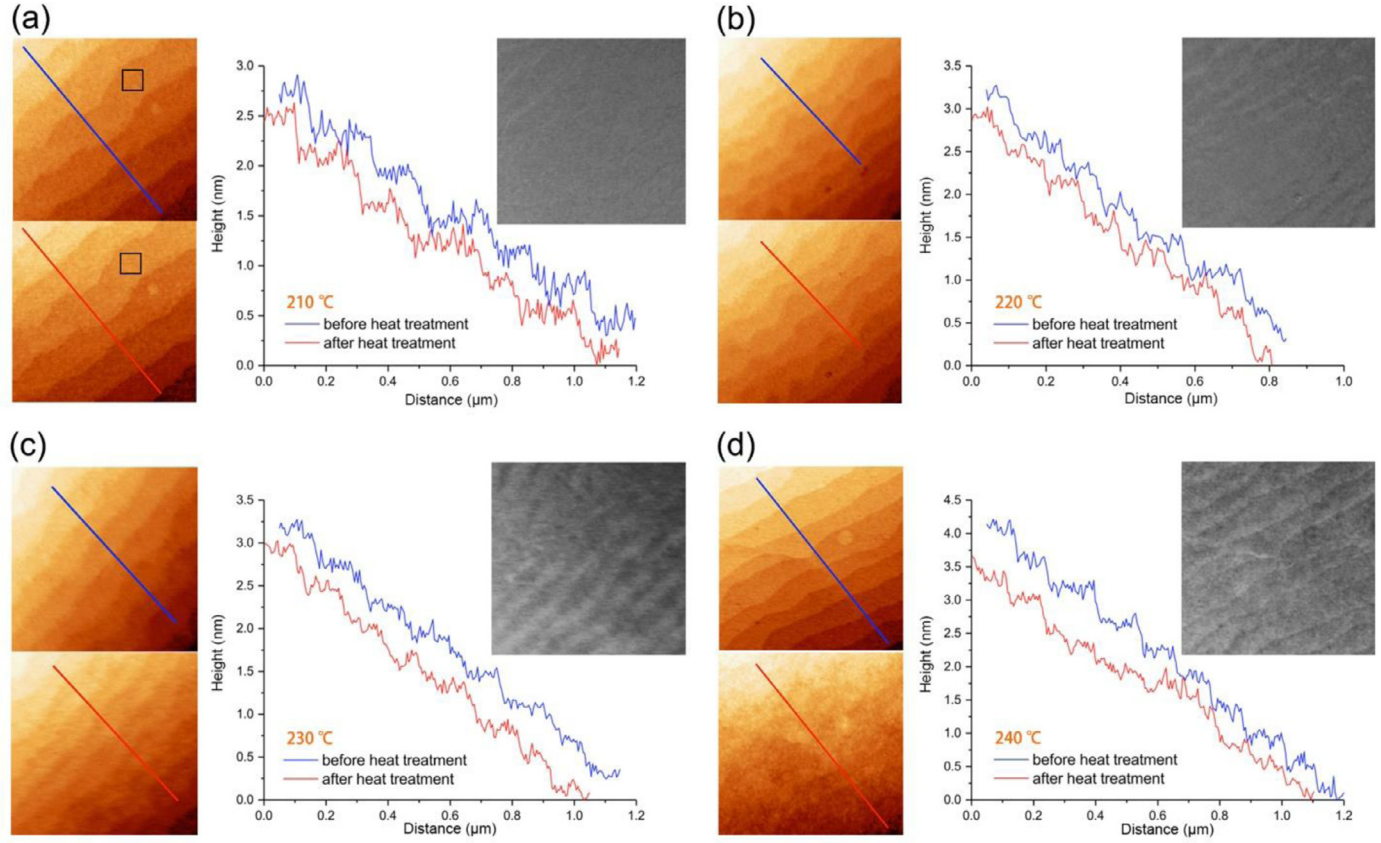

Fig. 3. Profile analysis of thermoplastically formed Pt-BMGs before and after heat treatment at (a) 210 °C, (b) 220 °C, (c) 230 °C and (d) 240 °C (samples were the same as in Fig. 2(b)–(e)). The before image (the top image on the left in each panel) and the after image (bottom) always represent the exact same location on the sample, the black-and-white image on the upper right is obtained by subtracting the before and after images from each other to highlight the locations where most changes occur, and the height profiles shown are taken at the location highlighted by the identically colored lines in the respective topographic images. All images are 1 μm × 1 μm in size. (For interpretation of the references to color in this figure legend, the reader is referred to the web version of this article.)

Table 1
Roughness ratios and relaxation times for samples treated between 210 °C and 250 °C. Relaxation times are calculated using parameters from Refs. [23,50].

Annealing temperature (°C)	210	220	230	240	250
Relaxation time	≈48 h	≈56 min	≈2 min	≈8.5 s	≈0.8 s
On-terrace roughness ratio	0.97 ± 0.05	1.00 ± 0.01	1.21 ± 0.10	1.59 ± 0.13	2.08 ± 0.51
Overall roughness ratio	0.96 ± 0.02	0.98 ± 0.01	1.00 ± 0.02	0.97 ± 0.01	2.68 ± 0.23

terraces, typically 100 nm × 100 nm, which ensures that they have no overlap with any of the step edges, leading to 'before' values of 0.55–0.95 Å with an average value around 0.8 Å. In contrast, areas to determine the overall roughness were 2 μm × 2 μm in size, which resulted in 'before' values of 0.6–0.9 Å.

Table 1 gives a chart of the two different ratios against treatment temperatures from 210 °C to 250 °C. Since it is impossible to identify the same location when the surface is blurred out after heated at 250 °C, the ratios for 250 °C are calculated from roughnesses obtained in similar areas sized identical to the ones used to calculate the roughness at the lower temperatures. For treatments at each temperature, the overall roughness ratio is the average of the ratios calculated for at least two different locations on the sample after plane subtraction had been applied on the raw data, and each of these locations contributes three squared and individually plane-subtracted areas towards the determination of the averaged on-terrace roughness ratios. As shown in the chart, the on-terrace ratio is, within the margin of error, unaffected for temperatures up to 220 °C, but then exposes significant on-terrace roughening. In contrast, the overall ratio remains almost the same (around 1.00) until the temperature reaches 250 °C.

The decrease of viscosity experienced when heated close – and eventually above – the material's glass transition temperature speeds up kinetics in BMGs, which results in two main effects as far as structural rearrangements on the surface are concerned. The first effect is the increase of the on-terrace roughness of the imprinted Pt-based BMG. This can be rationalized when recalling that the sample surface is forced into assuming virtually atomically flat, terraced structures during TPF. The atomic positions of surface atoms are therefore likely to be somewhat off the glass' lowest-energy state at the surface. As a result, the surface atoms will re-arrange and relax into a more stable, denser packed glass when provided with the mobility to do so by heating, which increases on-terrace roughness. This explanation fits well with the relaxation times as calculated with the Vogel–Fulcher–Tammann (VFT) relation [51–54] (cf. Table 1), which are for 210 °C and 220 °C much larger than the 20 min of annealing time, but is much shorter than this (2 min) at 230 °C, where surface roughening becomes first prominent. This is in particular interesting considering that

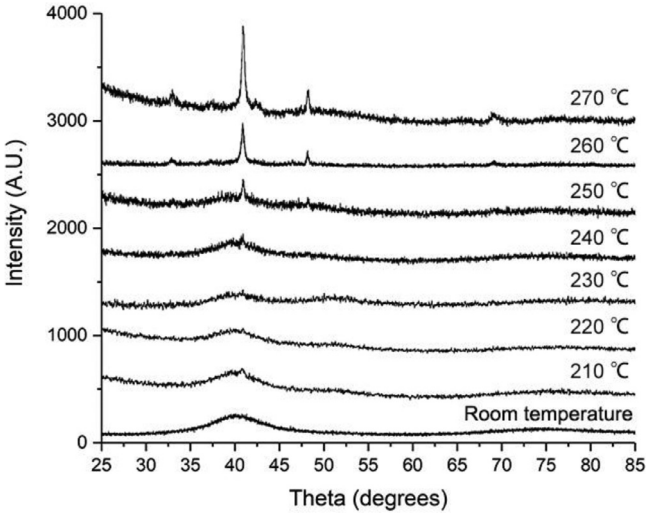

Fig. 4. X-ray diffraction spectra of samples made from Pt-BMG after being annealed for 20 min at temperatures from 210 °C to 270 °C, with the room temperature sample added for comparison.

one might reasonably expect surface kinetics to occur on a faster time scale than the bulk kinetics that the VFT relation describes [55]; the current observations, however, do not support such a conclusion, indicating that the roughening includes predominantly processes occurring below the surface. The competing effect is the trend to 'smoothen' the step edges, which arises because the step edges cause a larger surface energy compared to a flat surface. As a consequence, surface tension works towards eliminating the steps between the terraces as soon as the material's viscosity becomes low enough, similar to the mechanisms described in Ref. [56]. Both effects are obvious with the sample that was heated to 240 °C, i.e., right above T_g, which features blurred surfaces (Fig. 2(e)) and smoothened height profiles (Fig. 3(d)). Interestingly, the tendency to 'smoothen' the steps just about compensates the effect the increasingly rough surfaces of the terraces on have on the overall roughness value, resulting in an almost unchanged overall roughness even though the on-terrace roughness increases by ≈60%.

As the annealing temperatures rise further, the glass enters a regime where the atomic arrangement kinetics of the supercooled liquid becomes faster than the relaxation time. This enables not only higher mass transport in particular at the surface, but also aids nucleation and the subsequent growth of crystalline grains that results in larger and more corrugated surface features. For example, the samples heated at 250 °C lose all terraces but experience more than a doubling of their roughness. Complementary x-ray diffraction (XRD) spectra carried out on all eight samples (Fig. 4) confirm that the room temperature sample is fully amorphous (smooth spectra) while the samples heated to between 210 °C and 240 °C show the onset of a tiny peak, indicating that even though some ordering may have locally occurred, crystallization is overall still negligible. Then, at 250 °C, we see a clear peak despite the fact that the above-mentioned DSC measurements did not identify crystallization for the first hour. Finally, more and larger peaks are being detected for annealing temperatures of 260 °C and 270 °C, the latter in agreement with the earlier DSC results that finds such samples to be more than 95% crystalline. This trend coincides with observed increase of surface corrugation (Fig. 2(i)–(k)), which is why it makes sense to assign the related topographical changes at least in part to crystallization effects.

To summarize, this work presents a direct method of characterizing surface relaxation processes as well as the subsequent onset of crystallization for specially prepared samples made from a Pt-based BMG alloy. Thereby, the on-terrace roughness increase allows to directly quantify the impact of relaxation processes occurring near the sample's surface, which are found to occur on the same time scale as the ones expected for the bulk. This process is counteracted on a larger scale by the action of surface tension, which aims at smoothening out the step edges that separate individual terraces. When the temperature is raised to above 250 °C for a 20 min heat treatment, faster surface kinetics and crystallization become the dominating processes driving atomic rearrangements at the surface, which leads to a significant increase in surface corrugation. More generally, the new approach provides a unique way to investigate the relaxation of BMGs upon annealing, which can easily be combined with other methods such as mechanical, enthalpy, and density measurements.

Declaration of Competing Interest

The authors declare that they have no known competing financial interests or personal relationships that could have appeared to influence the work reported in this paper.

Acknowledgment

Funding by the Department of Energy through Grant no. DE-SC0016179 is gratefully acknowledged. Work carried out after 6/1/2019 was supported by the National Science Foundation Grant no. NSF CMMI-1901959. We thank the Alloy Behavior and Design Group at Oak Ridge National Laboratory for use of equipment.

Supplementary materials

Supplementary material associated with this article can be found, in the online version, at doi:10.1016/j.scriptamat.2020.02.035.

References

[1] C. Suryanarayana, A. Inoue, Bulk Metallic Glasses, CRC Press, 2011.
[2] M. Miller, P. Liaw, Bulk Metallic Glasses, Springer, New York, 2008.
[3] A.L. Greer, Science 267 (1995) 1947–1953.
[4] T.A. Waniuk, J. Schroers, W.L. Johnson, Appl. Phys. Lett. 78 (2001) 1213–1215.
[5] A. Inoue, W. Zhang, Appl. Phys. Lett. 83 (2003) 2351–2353.
[6] J. Schroers, JOM 57 (2005) 35–39.
[7] J. Schroers, N. Paton, Adv. Mater. Process. 164 (2006) 61–63.
[8] G. Kumar, H.X. Tang, J. Schroers, Nature 457 (2009) 868–872.
[9] J. Schroers, Adv. Mater. 22 (2010) 1566–1597.
[10] G. Duan, A. Wiest, M.L. Lind, J. Li, W.K. Rhim, W.L. Johnson, Adv. Mater. 19 (2007) 4272–4275.
[11] G. Kumar, A. Desai, J. Schroers, Adv. Mater. 23 (2010) 461–476.
[12] J. Schroers, T.M. Hodges, G. Kumar, H. Raman, A.J. Barnes, Q. Pham, T.A. Waniuk, Mater. Today 14 (2011) 14–19.
[13] M. Hasan, J. Schroers, G. Kumar, Nano Lett. 15 (2015) 963–968.
[14] G. Kumar, P.A. Staffier, J. Blawzdziewicz, U.D. Schwarz, J. Schroers, Appl. Phys. Lett. 97 (2010) 101907.
[15] J. Schroers, Phys. Today 66 (2013) 32–37.
[16] R. Li, Z. Chen, A. Datye, G.H. Simon, J. Ketkaew, E. Kinser, Z. Liu, C. Zhou, O.E. Dagdeviren, S. Sohn, J.P. Singer, C.O. Osuji, J. Schroers, U.D. Schwarz, Commun.Phys. 1 (2018) 75.
[17] M.E. Launey, R. Busch, J.J. Kruzic, Acta Mater. 56 (2008) 500–510.
[18] J.D. Ju, M. Atzmon, Acta Mater. 74 (2014) 183–188.
[19] J.C. Qiao, J.M. Pelletier, J. Mater. Sci. Technol. 30 (2014) 523–545.
[20] S.V. Ketov, Y.H. Sun, S. Nachum, Z. Lu, A. Checchi, A.R. Beraldin, H.Y. Bai, W.H. Wang, D.V. Louzguine-Luzgin, M.A. Carpenter, A.L. Greer, Nature 524 (2015) 200–203.
[21] W. Zhao, J.L. Cheng, H. Cheng, G. Li, Mater. Sci. and Eng. A 673 (2016) 239–242.
[22] T.C. Hufnagel, C.A. Schuh, M.L. Falk, Acta Mater. 109 (2016) 375–393.
[23] J. Ketkaew, W. Chen, H. Wang, A. Datye, M. Fan, G. Pereira, U.D. Schwarz, Z. Liu, R. Yamada, W. Dmowski, M.D. Shattuck, C.S. O'Hern, T. Egami, E. Bouchbinder, J. Schroers, Nat. Commun. 9 (2018) 3271.
[24] A. Datye, J. Ketkaew, J. Schroers, U.D. Schwarz, J. Alloys Compd. 819 (2020) 152979.
[25] R. Busch, J. Schroers, W.H. Wang, MRS Bull. 32 (2007) 620–623.
[26] A. Inoue, Mater. Sci. Eng. A 304–306 (2001) 1–10.

[27] Z. Chen, A. Datye, P.A. Brooks, M. Sprole, J. Ketkaew, S. Sohn, J. Schroers, U.D. Schwarz, MRS Adv. 4 (2019) 73–79.
[28] J. Tan, C.J. Li, Y.H. Jiang, R. Zhou, J. Eckert, in: Proceedings of the Eighth Pacific Rim International Congress on Advanced Materials and Processing, Cham, Springer, Cham, 2013, pp. 3199–3206.
[29] F. Zhu, H.K. Nguyen, S.X. Song, D.P.B. Aji, A. Hirata, H. Wang, K. Nakajima, M.W. Chen, Nat. Commun. 7 (2016) 11516.
[30] B. Huang, T.P. Ge, G.L. Liu, J.H. Luan, Q.F. He, Q.X. Yuan, W.X. Huang, K. Zhang, H.Y. Bai, C.H. Shek, C.T. Liu, Y. Yang, W.H. Wang, Acta Mater. 155 (2018) 69–79.
[31] R. Wiesendanger, M. Ringger, L. Rosenthaler, H.R. Hidber, P. Oelhafen, H. Rudin, H.-J. Güntherodt, Surf. Sci. 181 (1987) 46–54.
[32] B. Walz, R. Wiesendanger, L. Rosenthaler, H.-J. Güntherodt, M. Düggelin, R. Guggenheim, Mater. Sci. Eng. 99 (1988) 501–505.
[33] A. Zaluska, L. Zaluski, A. Witek, Mater. Sci. Eng. A 122 (1989) 251–255.
[34] T.M. Schaub, D.E. Bürgler, C.M. Schmidt, H.-J. Güntherodt, J. Non Cryst. Solids 207 (1996) 748–754.
[35] T.M. Schaub, D.E. Bürgler, H.-J. Güntherodt, EPL (Europhys. Lett.) 36 (1996) 601–606.
[36] B. Reinker, H. Geisler, M. Moske, K. Samwer, Thin Solid Films 275 (1996) 240–243.
[37] B. Reinker, M. Moske, K. Samwer, Phys. Rev. B 56 (1997) 9887–9893.
[38] D.E. Bürgler, C.M. Schmidt, D.M. Schaller, F. Meisinger, T.M. Schaub, A. Baratoff, H.-J. Güntherodt, Phys. Rev. B 59 (1999) 10895–10902.
[39] S. Ashtekar, G. Scott, J. Lyding, M. Gruebele, J. Phys. Chem. Lett. 1 (2010) 1941–1945.
[40] A.I. Oreshkin, N.S. Maslova, V.N. Mantsevich, S.I. Oreshkin, S.V. Savinov, V.I. Panov, D.V. Louzguine-Luzgin, Jetp Lett. 94 (2011) 58–62.
[41] A.I. Oreshkin, V.N. Mantsevich, S.V. Savinov, S.I. Oreshkin, V.I. Panov, N.S. Maslova, D.V. Louzguine-Luzgin, Appl. Phys. Lett. 101 (2012) 181601.
[42] A.I. Oreshkin, V.N. Mantsevich, S.V. Savinov, S.I. Oreshkin, V.I. Panov, A.R. Yavari, D.B. Miracle, D.V. Louzguine-Luzgin, Acta Mater. 61 (2013) 5216–5222.
[43] D.B. Miracle, Nat. Mater. 3 (2004) 697–702.
[44] D. Ma, A.D. Stoica, X.L. Wang, Nat. Mater. 8 (2008) 30–34.
[45] C. Fan, P.K. Liaw, C.T. Liu, Intermetallics 17 (2009) 86–87.
[46] A. Hirata, P. Guan, T. Fujita, Y. Hirotsu, A. Inoue, A.R. Yavari, T. Sakurai, M. Chen, Nat. Mater. 10 (2010) 28–33.
[47] Y.Q. Cheng, E. Ma, Prog. Mater. Sci. 56 (2011) 379–473.
[48] F. Zhu, A. Hirata, P. Liu, S. Song, Y. Tian, J. Han, T. Fujita, M. Chen, Phys. Rev. Lett. 119 (2017) 215501.
[49] J. Schroers, W.L. Johnson, Appl. Phys. Lett. 84 (2004) 3666–3668.
[50] B.A. Legg, J. Schroers, R. Busch, Acta Mater. 55 (2007) 1109–1116.
[51] H. Vogel, Physik. Zeitschr 22 (1921) 645–646.
[52] G.S. Fulcher, J. Ame. Ceram. Soc. 8 (1925) 339–355.
[53] G. Tammann, W. Hesse, Z. Anorg, Allg. Chem 156 (1926) 245–257.
[54] C.T. Moynihan, A.J. Easteal, M.A. De Bolt, J. Tucker, J. Am. Ceram. Soc. 59 (1976) 12–16.
[55] C.R. Daley, Z. Fakhraai, M.D. Ediger, J.A. Forrest, Soft Matter 8 (2012) 2206–2212.
[56] G. Kumar, J. Schroers, Appl. Phys. Lett. 92 (2008) 031901–031903.